HNPS Advances in Nuclear Physics

Vol 4 (1993)

HNPS1993

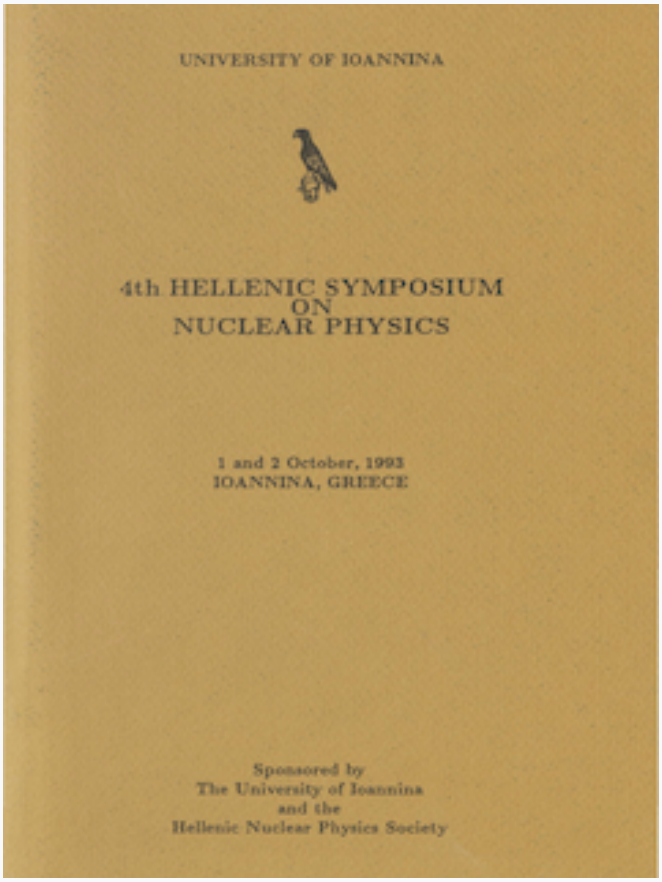

A Study of Greek Building Materials as Indoor Radon Sources

A. Savidou, C. Raptis, P. Kritidis

doi: 10.12681/hnps.2884

A STUDY OF GREEK BUILDING MATERIALS AS INDOOR RADON SOURCES

A. Savidou, C. Raptis and P. Kritidis

Institute of Nuclear Technology - Radiation Protection
National Centre for Scientific Research Demokritos, Athens, Greece

Abstract

A survey of radon emanation in building materials commonly used in Attica has initiated at our laboratory as part of a broader EU program. The objective is to obtain a characterisation of the Greek building materials as indoor radon sources and identify the cases where some specific countermeasures should be applied. Up to now, bricks commonly used in Attica have been studied for both radium content and radon emanation. Gamma-ray spectroscopy techniques, as well as radon exhalation measurements, have been employed. For determination of radon exhalation rate, besides the trivial method which consist of a single measurement of radon concentration in a closed vessel containing the sample, a short-time continuous accumulation/counting method has been established. The results of exhalation measurements have been used together with high-resolution gamma-spectrometry in order to determine radon emanation coefficients.

Introduction

Radon is a noble gas that belongs to the ^{235}U radioactive series. It is produced from ^{226}Ra decay and its half life is 3.8 days. The radon daughters are inhaled and become trapped in the lung, Short-lived radioactive decay products of radon delivering a radiation dose to the lung tissue. This dose eventually leads to lung cancer. According on NRPB 1989 47 per cent of the equivalent dose of the mean British citizen is related to radon inhalation (1).

Soil and building materials contain certain amounts of ^{226}Ra. After its decay radon is formed and a part of it diffuses into the surrounding air. The indoor radon concentrations are usually higher than outdoors due to radon accumulation in contrast with radon produced outdoor which can dissipate by air exchange processes.

Some typical radon concentrations are:

1. Countryside air, 2-8 Bq/m^3
2. Countryside air in the vicinity of uranium mines, up to 40 Bq/m^3
3. Dwellings air, 10-50 Bq/m^3 ,rarely higher than 500 Bq/m^3

The factors that influence the indoor radon concentrations are:

1. Properties of the building materials. The radon exhalation from building materials depends on the radium concentration, the density and porosity of the material.
2. Building construction. The indoor radon concentrations are influenced by the ventilation rate, which is strogly depends on the properties of the building, such as the use of insulating materials, artificial ventilation system etc.
3. Meteorological parameters. These may influence both the radon exhalation and the ventilation.

The objectives of our laboratory are:

1. Determination of radon emanation from building materials, which requires the knowledge of:
   a. Radium concentration
   b. Emanation coefficient
2. A study of various wall coating materials as mitigation media for radon exhalation rate.
3. Determination of the diffusion coefficients of radon diffusion in the materials.
4. Development of models for estimating the indoor radon concentrations.

Material and Methods

Brick samples have been collected from major local producers which represent eighty per cent of the total production in Attica.

Measurements of the specific activities in building materials

The specific activities of ^{226}Ra have been determined by use of low-background high-resolution gamma-spectrometry. The samples are powdered and closed in 75 cm^3 containers. These containers could be made gas-tight after closure so that radon could not escape from them. The samples are kept sealed for about 3 weeks before measurement so the radium, radon and its short-lived decay products reach radioactive equilibrium. The concentrations of ^{226}Ra are derived from the 295 keV and 352 keV photo peaks of ^{214}Pb and 609 keV photo peak of ^{214}Bi as the mean value of the results from these photo peaks. The 186 keV photo peak of ^{226}Ra is not used because of the interfering peak of ^{235}U, with energy of 185.7 keV. The counting time was 12000 s.

Measurements of the radon exhalation rate

For the radon exhalation rate measurements the samples is crushed into about 1 cm^3 particles in order to ensure that all radon that enters the pore space of the sample emanates into the chamber. An amount of about 300 gr of sample is used for each measurement.

a.closed vessel method

The closed vessel method has been used to measure the radon exhalation rate of the samples. The volume of the accumulation chamber is 1.2 l (Fig. 1). After a definite sealing time (20 h or 70 h or 96 h) , an amount of air is transferred from the accumulation chamber to a scintillation chamber by 10 min circulation that ensure uniform mixing. A filter is used to isolate the radon progeny. The alpha activity in the scintillation chamber is counted after three hours, to allow the equilibrium between radon and its daughters.

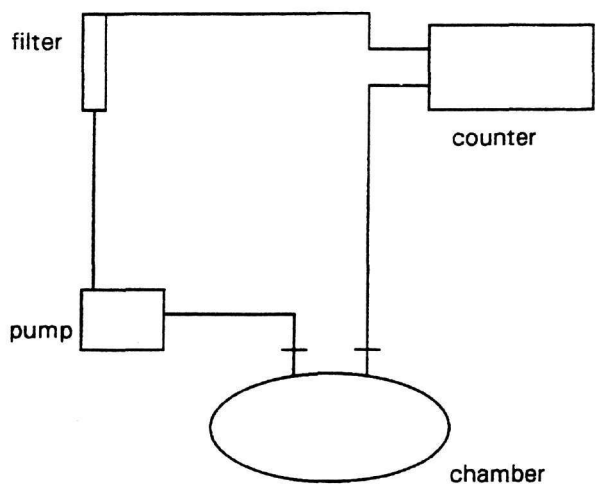

Figure 1. Schematic diagram of the closed vessel method.

The system has been calibrated by use of a thin ^{226}Ra standard with negligible reverse radon entry. The background of the detector is typically less than 2 cpm and the efficiency for detection of the alpha-particles of radon and its daughters is about 90 %. To ensure sealing silicon high vacuum grease is used. The comparison between the theoretical and the experimental data for radon decay confirms the absence of leakage . Five measurements have been made for each time interval of sealing. The results show that the total relative error of the method is less than 10 %.

b. continuous accumulation/counting method

The measuring system is the same as in the closed vessel method, but in this case the air is circulating continuously and the counting is continuous as well. The concentration of radon and its daughters in the scintillation chamber increases with time. The accumulating counts are proportional to the time integral of the total alpha-activity in the chamber. a thin ^{226}Ra standard is used for calibration . The advantage of the method is the shorter accumulation period, which results in reduced influence of the reverse entry process (2). Only a few hours of circulation are needed to determine the exhalation rate of a typical sample. The monitoring of the reverse entry process is possible by comparing the experimental data in consequent times with those derived by use of a thin ^{226}Ra standard. When the reverse effect is negligible the ration of sample counts to the standard source counts after a certain period of time is given by the formula:

$$\frac{C_{spl}}{C_{src}} = \frac{b_{spl} \cdot q_{spl}}{b_{src} \cdot q_{src}}$$

were:

C_{spl}, C_{src}: the counts after sample and source measurement

b_{spl}, b_{src}: the ration of the scintillation chamber volume to the available volume for the sample and the source respectively

q_{spl}, q_{src}: The emanation rates of the sample and source

The first experimental results for bricks indicated a significant presence of thoron in the measuring chamber. Thoron half life is 55.6 s while this of radon is quite higher 3.82 d. When the brick sample is measured the alpha-count integral is linear with time in contrast with the calibration curve obtained with the thin ^{226}Ra source. This indicates that the number of alpha-decay nuclei in the vessel remains stable. Due to its low half life, thoron concentration in the vessel is stabilised a few minutes after sealing. So the alpha-counts integral linearity seems to be related with thoron. The integral of alpha-counts as a function of time in the case of the continuous accumulation/counting measurements, is shown in fig.2, including the calibration curve, those of a radium mineral and a brick sample as well as the theoretical curve

corresponding to the thin radium source. The alpha-counts integral for the radium rich mineral and for the source are quite close to the theoretical curve.

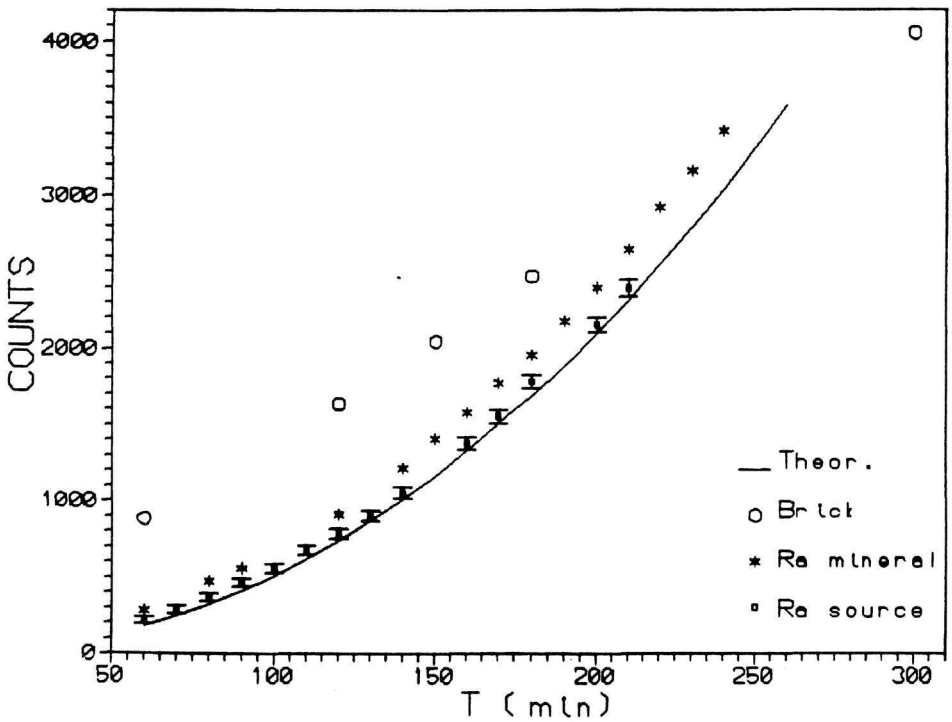

Figure 2 : The integral of alpha-counts as a function of time in the case of the continuous accumulation/counting measurements.

To eliminate thoron contribution of measurements in building materials, physical methods are planned to be used.

The continuous accumulation/counting method will be particularly suitable in the case of samples with high exhalation rate, e.g. concrete.

Results

The radium concentration, the specific exhalation rate and the emanation coefficient for six brick samples are given in the Table 1. The values, indicate that the radium content of bricks alone cannot be used to evaluate the exhalation rate of radon . The specific exhalation rate has been determined by the closed vessel method.

TABLE 1

MEASUREMENTS OF BRICK SAMPLES

Ra Bq/Kgr	Rn 10^{-3} Bq/h.Kgr	n %
26 ± 4	13 ± 3	6 ± 1
33 ± 4	42 ± 4	17 ± 2
34 ± 4	7 ± 3	2 ± 1
35 ± 4	4 ± 2	1.6 ± .8
33 ± 4	3 ± 1	1.1 ± .3
83 ± 5	9 ± 3	1.4 ± .5

The values in Table 1 can be compared with those reported for bricks from Netherlands, Belgium and USA, as summarised in Table 2.

TABLE 2

REPORTED RESULTS FOR BRICKS FROM OTHER COUNTRIES

	Rn 10^{-3} Bq/h.Kgr	n %
Netherlands (3)	3.4 29	1.2 -
Belgium (4)	0.8 - 6.5	0.1 -2.2
USA (5)	3.7	1

REFERENCES

1. The National Radiological Protection Board, 'Living with Radiation', United Kingdom, 1989.
2. L. Morawska, Health Physics Vol. 57, No.3, pp.481-483, 1989.
3. W. van Dijk and P. de Jong, Health Physics Vol. 61, No.4, pp. 501-509, 1991.
4. Poffijn et al., Radiat. Prot. Dosim. Vol. 7, pp. 77-79, 1984.
5. Ingersoll, J. G. , Health Physics Vol. 45, pp. 363-368, 1983.

THE DECAY OF ^{164}Yb* FORMED IN ASYMMETRIC AND NEARLY SYMMETRIC FUSION REACTIONS

N.G. Nicolis[a], J.L. Barreto[b], D.G. Sarantites, R.J. Charity, L.G. Sobotka, and D.W. Stracener

Washington University, St. Louis, Missouri 63130, U.S.A.

D.C. Hensley, J.R. Beene, M. Halbert, C. Baktash and M. Thoennessen[c]

Oak Ridge National Laboratory Oak Ridge, Tennessee 37830, U.S.A.

ABSTRACT

The decay of ^{164}Yb*, formed at E* $\approx$ 54 MeV in ^{16}O + ^{148}Sm and ^{64}Ni + ^{100}Mo reactions is investigated. Evaporation residue cross sections, entry state γ-ray fold distributions as well as energy and angular distributions of exit-channel selected charged particles were obtained for each reaction, using 4π detection systems for both particles and γ-rays. A projectile breakup mechanism was identified in the ^{16}O-induced reaction that affects the population of the αxn evaporation residue channels. Observed differences in the γ-ray fold distributions of the xn channels of the two reactions are interpreted in terms of differences in the compound nucleus spin distributions in each case. An analysis of fusion and evaporation residue excitation functions is also made in an energy range from near to well below the entrance channel Coulomb barrier, for both reactions. A comparison of the exit channel fractional cross sections of the xn channels shows trends that correlate with the behaviour of the low and high spin regions of the primary spin distributions.

The statistical model of nuclear reactions, based on the Bohr independence hypothesis, has been quite successful in describing a large volume of experimental data concerning the decay of compound nuclei formed in heavy-ion fusion [1]. Despite this success, some studies have questioned the Bohr hypothesis because of an apparent failure of the model to account for certain reaction characteristics. In particular, an unexpected dependence of the compound nucleus decay on the mode of formation was reported a few years ago [2]. Ruckelshausen et al. [2], performed measurements of evaporation residue angular momentum distributions using the Heidelberg Crystal Ball. The decay of the ^{156}Er compound nucleus produced at the excitation energy of 47 MeV was studied in a cross bombardment of ^{12}C + ^{144}Sm and ^{64}Ni + ^{92}Zr. Strong differences in the αxn and high spin xn populations were observed. For the xn channels, in particular, the ratio of the 2n/3n cross sections as a function of the compound nucleus spin was found to depend on the entrance channel, suggesting that there is memory of the mode of formation in the particle evaporation process.

In order to shed some light on this subject, we performed a detailed study of the

decay of the nearby compound nucleus ^{164}Yb* formed at the initial excitation energy of E* $\approx$ 54 MeV in the reactions ^{16}O + ^{148}Sm and ^{64}Ni + ^{100}Mo [3]. The experiment was performed at the Holifield Heavy-Ion Research Facility at the Oak Ridge National Laboratory. Energy and angular distributions of the light charged particles (p, d, ^{3}He, α) emitted in these reactions were measured with the Dwarf Ball. The Dwarf Ball, a nearly 4π CsI(Tl) scintillator array [4], consists of 70 equal solid angle detectors covering laboratory angles from θ_{lab} = 12° to 168°. Furthermore, evaporation residue γ-ray fold distributions and total γ-ray information, in a nearly 4π geometry, were obtained with the Oak Ridge Spin Spectrometer [5]. The above measurements were made in coincidence with discrete γ-transitions in the evaporation residues detected with 18 Compton-suppressed Ge detectors that replaced 18 of the 70 NaI detectors of the Spin Spectrometer. The experimental setup provided a complete set of particle and γ-ray measurements for the comparison of the two reaction systems.

The data reduction procedures described in Ref. [3] yielded the energy and angular distributions of the emitted protons and α-particles in coincidence with discrete γ-transitions in the evaporation residues. The γ-ray fold distributions resulting after xn (x=2, 3, 4 and 5) and α2n, α3n evaporation were compared for the two reactions. The comparison of the xn fold distributions is facilitated by considering the cross section ratios $\sigma_i(k_{eff})/\Sigma\sigma_i(k_{eff})$, where i=2, 3, 4, 5n and k_{eff} is the effective γ-ray fold [3]. The experimental cross section ratios are plotted in Fig. 1(a) as a function of k_{eff}. The open symbols refer to the ^{16}O + ^{148}Sm and the closed ones to the ^{64}Ni + ^{100}Mo reaction. Different decay channels are denoted by the symbols shown in the figure. For the decay channels observed in both reactions, we observe a shift in the cross section ratios by $\sim$ 2 units down in k_{eff} for the ^{64}Ni-compared to the ^{16}O-induced reaction. The γ-ray fold distributions of the α2n and α3n channels are shown in Figs. 1(b) and (c). In these distributions we observe an opposite trend, namely, a downward shift in k_{eff} by $\sim$ 2 units for the ^{16}O + ^{148}Sm distributions with respect to ^{64}Ni + ^{100}Mo. The above trends are in similar to the ones reported in Ref. [2].

Important information for the understanding of the αxn decay of ^{164}Yb* resulted from the analysis of the energy and angular distributions of the emitted α-particles. The histograms in Fig. 2 show the α-particle CM spectra, for selected angles, in coincidence with the $2^+ \rightarrow 0^+$ transition in ^{158}Er (α2n), for both reactions. We note that in the ^{64}Ni + ^{100}Mo reaction the shapes of the forward and backward spectra are similar. However, in ^{16}O + ^{148}Sm, the forward spectra are considerably more energetic than the backward ones. Statistical model calculations that describe closely the measured evaporation residue cross sections provide a good description of the shapes and absolute magnitude of the spectra for ^{64}Ni + ^{100}Mo and make evident the existence of a high energy component in the forward direction for ^{16}O + ^{148}Sm (dashed lines in Fig. 2). It was established [3] that the forward emitted energetic α's (Fig. 2(a)) correspond to low γ-ray folds. This non-equilibrium component was associated with an incomplete fusion process in which the ^{16}O projectile breaks up into ^{12}C + α, followed by fusion of the ^{12}C with the target nucleus. The subsequent decay of the resulting ^{160}Er* by 2 or 3 neutron emission contributes to the α2n and α3n channels under study. This results in shifts of the γ-ray multiplicity distributions

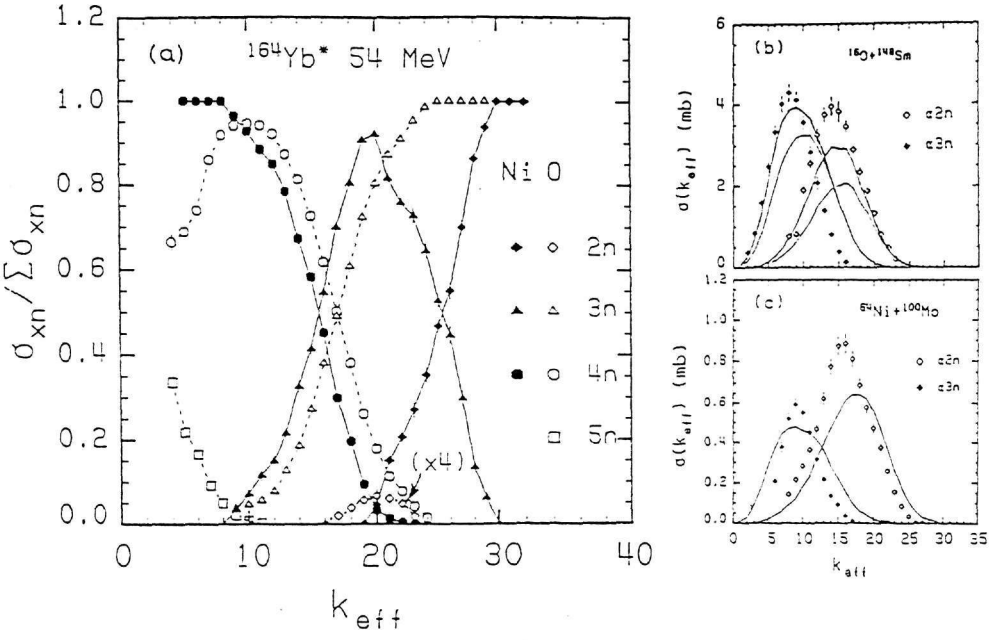

Fig. 1. (a) Cross section ratios $\sigma_i(k)/\Sigma\sigma_i(k)$ as a function of the effective γ-ray fold, k_{eff}, for the 2n, 3n, 4n and 5n channels. Solid symbols refer to the ^{64}Ni + ^{100}Mo and the open symbols to the ^{16}O + ^{148}Sm reaction. The lines guide the eye. (b),(c) Experimental γ-ray fold distributions (symbols) associated with the α2n and α3n decay channels in ^{16}O + ^{148}Sm and ^{64}Ni + ^{100}Mo reactions. The lines represent the results of statistical model calculations.

to values lower than those associated with the equilibrium decay of ^{164}Yb* This finding provides a rational explanation to the previously reported differences in the evaporation residue spin distributions involving αxn emission [2]. In the study of Ruckelshausen et al. [2], the strongest entrance channel mass asymmetry was achieved in ^{12}C-bombardments; i.e. a projectile that could also lead to incomplete fusion.

The extent to which the data can be described in terms of decays from an equilibrated compound nucleus was examined with statistical model calculations performed with the code EVAP [6]. It was assumed that the only difference in the compound nucleus decay arrises from the primary angular momentum distributions, σ_ℓ, in each reaction. For the ^{16}O + ^{148}Sm reaction, the σ_ℓ-distributions were deduced from an one-dimensional barrier penetration model calculation. For ^{64}Ni + ^{100}Mo, σ_ℓ was extracted from a simplified coupled-channels calculation with the code CCFUS [8,9]. The code takes into account the effect of coupling of the entrance channel to various inelastic and transfer degrees of freedom in the projectile and target. Starting with a primary σ_ℓ distribution, the code EVAP calculated the evaporation residue entry state distributions (I_{ER}) and the corresponding

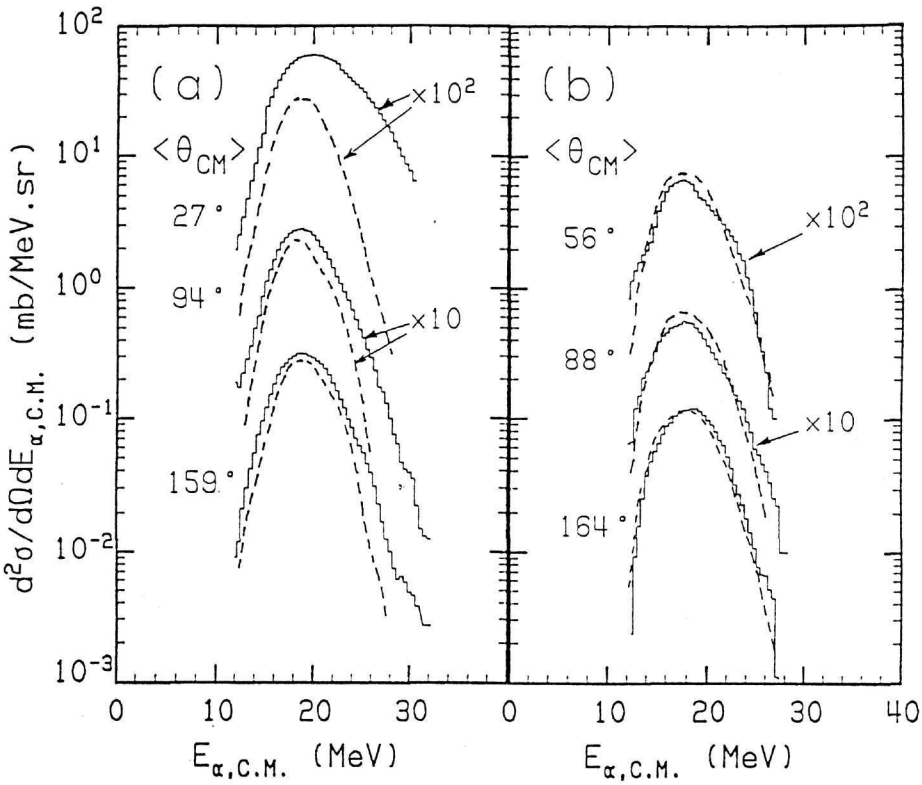

Fig. 2. The histograms show the observed energy spectra of α-particles associated with the α2n exit channel, at the indicated center of mass angles, for (a) the ^{16}O + ^{148}Sm and (b) the ^{64}Ni + ^{100}Mo reaction. The dashed lines show the corresponding spectra calculated assuming emission from an equilibrated ^{164}Yb* compound nucleus.

γ-ray multiplicity distributions (M_γ). The M_γ-distributions were folded with the Spin Spectrometer response function to produce the k_γ-distributions to be compared with the experimental data. The folding method was found preferable to the unfolding used in Ref. [2], i.e. $k_\gamma \rightarrow M_\gamma \rightarrow I_{ER} \rightarrow \ell$.

The comparison of the xn cross section ratios as a function of k_{eff} with the results of the calculation is made in Fig. 3. The ratios for the ^{16}O + ^{148}Sm reaction are well reproduced. For ^{64}Ni + ^{100}Mo, the agreement below $k_{eff} \sim 20$ is also good. The underprediction of the 2n and overprediction of the 3n high k_γ ratios is attributed to uncertainties in the coupling strengths in the calculation of σ_ℓ. The evaporation calculation for the fold distributions of the α2n and α3n channels is shown by the thin lines in Fig. 1(b) and (c). For ^{16}O + ^{148}Sm, the calculated distributions peak at a higher fold than the experimental ones. The previously mentioned incomplete fusion mechanism was simulated using the model of

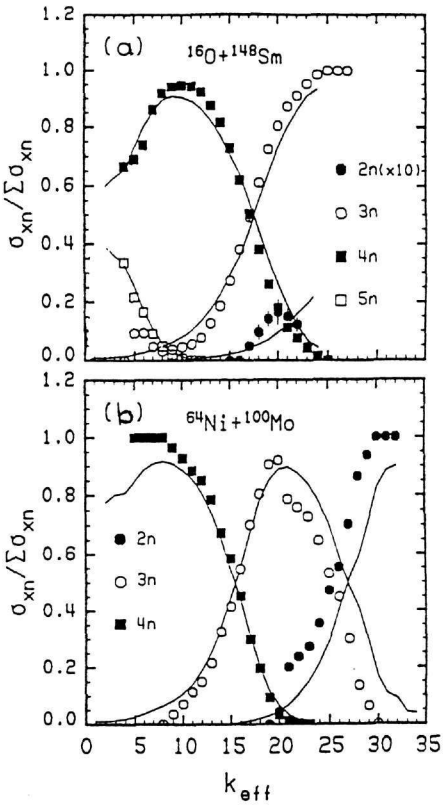

Fig. 3. (a) Comparison between the experimental (symbols) and calculated (solid curves) cross section ratios of the indicated xn channels versus the effective γ-ray fold, for the ^{16}O + ^{148}Sm reaction. (b) Same as in (a), for ^{64}Ni + ^{100}Mo.

Wilczyński et al. [7] and the decay of the resulting $^{160}Er^*$ was calculated with the statistical model. Adding the 2n and 3n contributions to the α2n and α3n channels (originating from the equilibrium decay of $^{164}Yb^*$) produces the distributions shown by the thick curves in Fig. 1(b). This leads to a substantial improvement in the description of the data.

Therefore, we conclude that no reason other than the incomplete fusion mechanism found in ^{16}O + ^{148}Sm and the difference in the primary spin distributions is responsible for the observed differences in the decay of $^{164}Yb^*$ populated in the two reactions.

The comparison of the reduced spin distributions $\sigma_\ell/\pi\lambda^2$ employed in the statistical model calculations is made in Fig. 4. The distributions of the two reactions calculated with the one-dimensional barrier penetration model are shown by the curves labelled ^{16}O and ^{64}Ni uncoupled. The distribution labelled coupled includes the effect of coupling to the low lying collective excitations plus additional transfer couplings in ^{64}Ni + ^{100}Mo interactions

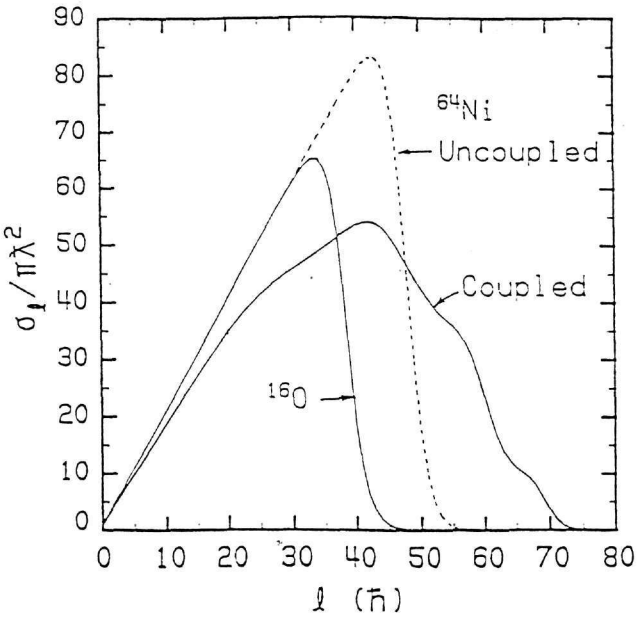

Fig. 4. Reduced spin distributions for the two reactions calculated with the one-dimensional barrier penetration model (curves labelled ^{16}O and ^{64}Ni uncoupled). For the ^{64}Ni-induced reaction, the effect of coupling to inelastic and transfer degrees of freedom is shown by the curve labelled coupled.

[3]. Compared with the one of the ^{16}O-induced reaction, it shows a suppression of the low and an enhancement of the high-ℓ partial waves. This has a prominent effect in the compound nucleus decay by neutron evaporation. The fractional cross sections of the xn channels originating from high spin states (small x) in the mass symmetric reaction has to be greater than the one in the asymmetric reaction. Similarly, there should be a suppression of fractional cross sections of the low spin channels (large x) in the mass symmetric reaction.

This effect was demonstrated in an analysis of compiled evaporation residue excitation function data for the two reactions [10]. In Fig. 5, the experimental decay fractions of the xn channels (defined as the ratio of a partial to the total evaporation residue cross section) are plotted as a function of the compound nucleus excitation energy. Open symbols refer to the ^{16}O + ^{148}Sm [3,11] and the closed ones to the ^{64}Ni + ^{100}Mo [3,12] reaction. Squares, circles and triangles correspond to the 2n, 3n and 4n channels, respectively. In the ^{16}O-induced reaction, the 2n decay fraction decreases monotonically with increasing excitation energy E*. The 3n fraction increases initially with E*, attains a maximum at 38 MeV and then decreases. The 4n fraction shows a monotonic increase with E*. In the ^{64}Ni-induced reaction, the trend of the corresponding decay fractions with E* is essentially the same. However, there are striking differences when compared with the fractions of the ^{16}O-

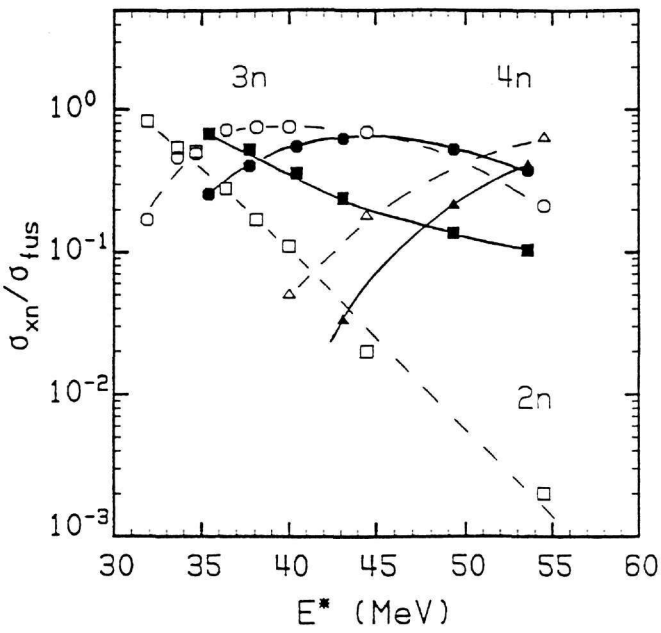

Fig. 5. Experimental decay fractions of ^{164}Yb* formed in the fusion of ^{16}O + ^{148}Sm and ^{64}Ni + ^{100}Mo (open and closed symbols) as a function of the compound nucleus excitation energy. Evaporation residue channels involving emission of 2, 3 and 4 neutrons are indicated with squares, circles and triangles. The lines guide the eye.

induced reaction. We observe a significant enhancement of the 2n fraction which persists throughout the excitation energy range. The 3n fraction shows a suppression at low E* and an enhancement above 48 MeV, where it peaks. Finally, the 4n fraction is suppressed in the whole excitation energy range. Due to the fact that both data sets are plotted with the compound nucleus excitation energy as a common abscissa, we attribute the observed differences to the populated compound nucleus states in each reaction.

Next, we examine the extent to which the evaporation residue data are described with statistical model calculations employing σ_ℓ distributions from models that describe closely the measured fusion excitation functions. The closed symbols in Fig. 6 show the measured fusion cross sections in the two reactions. The fusion model predictions are given by the solid curves. The ^{16}O + ^{148}Sm excitation function is described well with a variation of an one-dimensional barrier penetration model [10]. In ^{64}Ni + ^{100}Mo, the calculation with CCFUS interpolates between the high energy points and provides a good description of the cross sections in the subbarrier region. It also provides a good description of the energy dependence of the moments of the measured spin distributions [10]. The evaporation residue excitation function data of the 2n, 3n and 4n channels are shown by the squares, circles and triangles in Fig. 6. They are compared with the results of the statistical model

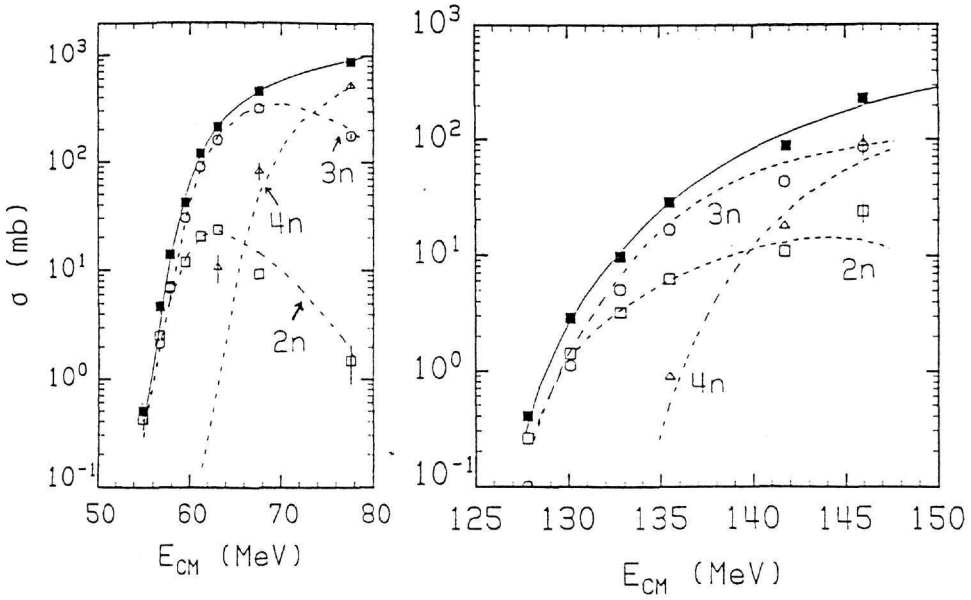

Fig. 6. (a) Measured evaporation residue cross sections of the indicated xn channels (open symbols) and total cross section (closed symbols) as a function of the center of mass energy for $^{16}O + ^{148}Sm$. Calculated excitation functions are shown by the solid and dashed lines. (b) Same as (a), for $^{64}Ni + ^{100}Mo$.

calculation shown with the dashed curves. The majority of the data is described well using the same statistical model parameters, the only difference being the employed σ_ℓ distributions in each reaction. Some of the discrepancies in the description of the $^{64}Ni + ^{100}Mo$ reaction are associated with the lack of a sufficient number of fusion measurements, especially in the above the Coulomb barrier energy region.

Summarizing, the decay of $^{164}Yb^*$ formed in a nearly mass symmetric ($^{64}Ni + ^{100}Mo$) and an asymmetric ($^{16}O + ^{148}Sm$) fusion reactions was studied. Both the detailed study at $E^* = 54$ MeV and the study of the two reactions as a function of E^* reveals differences which can be associated with the population of a broad spin distribution in the ^{64}Ni-induced reaction. In the statistical model description of the compound nucleus decay, it was assumed that the only difference in the formation of $^{164}Yb^*$ in the two reactions arrises in the σ_ℓ distributions which are quite different according to the predictions of current fusion models. Based on this assumption, most of the experimental features were essentially understood without the need to resort to strong structural influences on the deexcitation of the compound nucleus by particle emission.

This work was supported by the Director, Office of Energy Research, Office of High Energy and Nuclear Physics, Nuclear Physics Division of the US Department of Energy, under contract Nos. DE-FG02-87-ER40316 and DE-FG02-88-ER40406. Oak Ridge National Laboratory is managed by Martin Marietta Energy System, Inc. under Contract No. DE-AC05-84OR21400 with the Department of Energy.

[a] Department of Physics, University of Ioannina, Ioannina 45110, GREECE.
[b] On leave from Instituto de Física da UFRJ - CP 21945 - RJ, BRAZIL.
[c] NSCL, Michigan State University, East Lansing, Michigan 48824.

REFERENCES

[1] R.G. Stokstad, in *Treatise on Heavy-Ion Science* (Plenum Press, N.Y. 1985) Vol.3, p.83.

[2] A. Ruckelshausen, R.D. Fischer, W. Kühn, V. Metag, R. Mühlhans, R. Novotny, T.L. Khoo, R.V.F. Janssens, H. Gröger, D. Habs, H.W. Heyng, R. Repnow, D. Schwalm, G. Duchène, R.M. Freeman, B. Haas, F. Haas, S. Hlavac, and R.S. Simon, Phys. Rev. Lett. **56**, 2356(1986); A. Ruckelshausen et al., Phys. Rev. Lett. **58**, 1584(1987).

[3] J.L. Barreto, N.G. Nicolis, D.G. Sarantites, R.J. Charity, L.G. Sobotka and D.W. Stracener, D.C. Hensley, J.R. Beene, C. Baktash, M. Halbert and M. Thoennessen, (Accepted for publication in Phys. Rev. C).

[4] D.W. Stracener, D.G. Sarantites, L.G. Sobotka, J. Elson, J.T. Hood, Z. Majka, V. Abenante, A. Chbihi and D.C. Hensley, Nucl. Inst. Meth. **A294**, 485(1990).

[5] M. Jääskeläinen, D.G. Sarantites, R. Woodward, F.A. Dilmanian, J.T. Hood, R. Jääskeläinen, D.C. Hensley, M. Halbert and J.H. Barker, Nucl. Inst. Meth. **204**, 385(1983).

[6] Statistical model evaporation code EVAP. N.G. Nicolis, D.G. Sarantites and J.R. Beene (to be published).

[7] J. Wilczyński, K. Siwek-Wilczyńska, J. Van Driel, S. Gonggrijp, D.C.J.M. Hageman, R.V.F. Janssens, J. Lukasiak, R.H. Siemssen and S.Y. Van der Werf, Nucl. Phys. A**373**, 109(1982).

[8] S. Landowne and C.H. Dasso, Phys. Lett. **138**B, 32(1984).

[9] C.H. Dasso and S. Landowne, Comput. Phys. Commun. **46**, 187(1987).

[10] N.G. Nicolis and D.G. Sarantites, (Accepted for publication in Phys. Rev. C)

[11] D.E. DiGregorio, M. diTada, D. Abriola, M. Elgue, A. Etchegoyen, J.O. Fernández Niello, A.M.J. Ferrero, S. Gil, A.O. Macchiavelli, A.J. Pacheco, J.E. Testoni, P.R. Silveira Gomes, V.R. Vanin, R. Liguori Neto, E. Crema and R.G. Stokstad, Phys. Rev. C**39**, 516(1989).

[12] M.L. Halbert, J.R. Beene, D.C. Hensley, K. Honkanen, T.M. Semkow, V. Abenante, D.G. Sarantites, and Z. Li, Phys. Rev. C **40**, 2558(1989).